Journal Name

Dynamic Article Links ►

Cite this: DOI: 10.1039/c0xx00000x

www.rsc.org/xxxxxx

ARTICLE TYPE

Organic Solar Cells Based on Nanoporous P3HT Obtained from Self Assembled P3HT:PS Templates†‡

Varun Vohra,*[a] Mariano Campoy-Quiles,[b] Miquel Garriga[b] and Hideyuki Murata*[a]

Received (in XXX, XXX) Xth XXXXXXXXX 20XX, Accepted Xth XXXXXXXXX 20XX

DOI: 10.1039/b000000x

We demonstrate a solution-based method to create vertical nanoporous structures of semiconducting polymer poly(3-hexylthiophene) over large areas by taking advantage of the spontaneous phase segregation between poly(3-hexylthiophene) and polystyrene deposited from a single solution and, in a second step, removing polystyrene by selectively dissolving it. Nanoporous films with pore diameters which can be tuned down to 120 nm are produced by varying the composition. The potential of the method is further demonstrated by fabricating fully operational solar cells after deposition of [6,6]-phenyl-C61-butyric acid methyl ester from an adequate solvent. For optimized conditions, the devices based on nanostructured thin films exhibit enhanced efficiencies with respect to graded bilayers and bulk heterojunction organic photovoltaic devices. We relate the increase in fill factor observed in the nanostructured devices to changes in the orientation of poly(3-hexylthiophene) chains induced by nanoconfinement and self assembly with polystyrene resulting from this simple solution process without any use of elaborated chemistry or soft lithography.

Introduction

The scientific community has shown increasing interest in conjugated polymer solar cells since the introduction of donor acceptor systems based on poly(3-hexylthiophene) (P3HT) and fullerene derivatives such as [6,6]-phenyl-C61-butyric acid methyl ester (PCBM).[1-4] The P3HT – PCBM bulk heterojunction solar cells, reaching over 5 % of efficiency, has become the reference in the field of polymer photovoltaics.[5,6] Although such architectures allow intimate mixing of both materials leading to very efficient photoinduced charge separation, the charges cannot always find a percolation path to reach the respective electrodes. Along with different post process treatments such as thermal[5,6] and solvent[7] annealing, alternative structures have been studied to increase the charge collection and decrease the recombination rate within the active layers of the polymer solar cells by modifying the nanostructure of the active layer. Among these, vertical composition gradients[8-11] and interdigitated nanostructures[12,13] have been of a particular interest as they are believed to be the optimum heterojunction nanostructure. By spin coating PCBM from a dichloromethane solution on top of a P3HT layer, the diffusion of PCBM into the pure P3HT underlying layer produces devices with a vertical composition profile and similar efficiencies with respect to the bulk heterojunctions.[9-11]

On the other hand, intensive research has been ongoing to obtain an efficient method to produce nanostructured conjugated polymers such as P3HT.[12-17] These include nanoimprinting using soft replica of regular nanostructures obtained from self assembled structures such as porous alumina[12-14] and methods based on specifically designed polymers or block copolymers.[15-17] Confining the P3HT chains in nanostructures such as nanopillars obtained using porous alumina,[14] for instance, can induce orientation of the P3HT chains with the polymer backbone lying parallel to the substrate resulting in an increase of the device performance. However, even though such methods can lead to very well organized structures, each of them presents some drawbacks. The formation of hexagonally arranged pores on alumina involves complicated mechanisms, specific instrumentation and is time consuming. In addition, the replication procedure of these structures through nanoimprinting is a time-consuming, multistep method that requires very high control of the process parameters (applied pressure, temperature and time) to perfectly replicate the nanostructures, especially on the submicrometer scale. In very recent literature, the idea of using phase segregation and further removing one of the polymers has been proposed. However, the structures either require the synthesis of new elaborated polymers[15-17] or use commercially available low efficiency donor materials.[18]

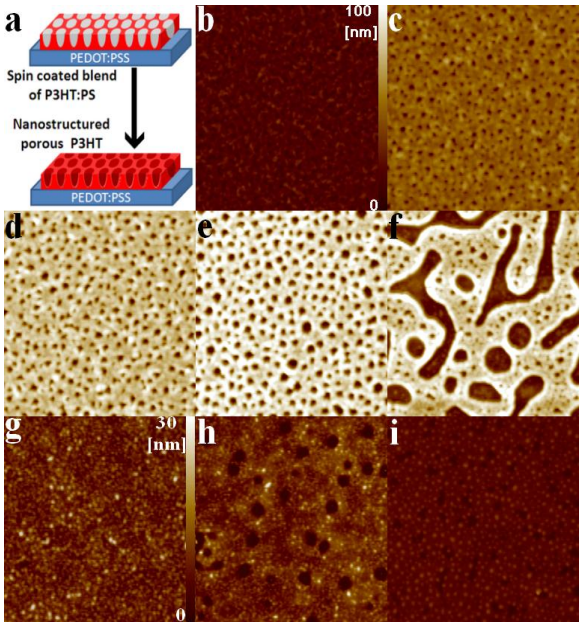

Figure 1. (a) Schematic representation of the phase segregated spin coated film of P3HT:PS before and after soaking into acetone for 30 min (red and grey domains correspond respectively to P3HT and PS); AFM images after PS removal of films obtained with 0 (b), 15 (c), 25 (d), 35 (e), 50 (f), 65 (g), 75 (h) and 85 (i) wt% of PS blended with P3HT; image area is 10μm x 10μm; the z-axis scale (displayed in (b)) applies to (b) to (f) images, and that on (g) applies to (g), (h) and (i).

We hereby present a simple method based on self organized phase segregation between two polymers, namely P3HT and polystyrene (PS), to produce nanoporous P3HT thin films directly on a poly(3,4-ethylenedioxythiophene) poly(styrenesulfonate) (PEDOT:PSS) covered Indium Tin Oxide (ITO) substrate. Combining the potential benefits of direct nanostructuration and sequential solution processing, we create active layers with a vertical composition profile and a predefined nanostructure. P3HT is a well known commercially available polymer that exhibits good photovoltaic performances when combined with fullerene derivatives such as PCBM. Moreover, PCBM is deposited on these nanostructured P3HT films from dichloromethane leading to photovoltaic devices which exhibit higher device performances with respect to graded bilayer and bulk heterojunction solar cells prepared in our laboratory. This method therefore offers a very easy and convenient way to obtain devices with power conversion efficiencies reaching up to 3.25% or increasing the fill factors up to 56%. Using advanced ellipsometric characterization[19] combined with Fourier Transform Infrared spectroscopy (FTIR), we find that, unlike what was seen in previous works on nanostructure formation through phase segregation between two polymers, the enhancement of the device performances is not only related to the increase of interface between donor and acceptor but also to molecular orientation induced by nanoconfinement and interaction between the two phase separated polymers. Such molecular orientation of the P3HT chains leads to very efficient charge separation and collection.

Results and Discussion

Phase segregation between two polymers depends considerably on the relative concentration of each of the polymers in the blend as defined by their phase diagram. In previous studies, it has been demonstrated that the difference in solubility of PS and Polyalkylthiophenes in solvents such as chlorobenzene can lead to self assembled film architectures containing PS-rich and Polyalkylthiophene-rich domains readily after film deposition.[20] During the spin coating process of P3HT blended with PS, well defined phase separated domains of P3HT and PS can be formed. As acetone is a solvent for PS but not for P3HT, it can be used to selectively remove the PS domains from the phase separated films.

In Figure 1, a schematic representation of the film after spin coating and after removing the PS is displayed along with the structures that can be obtained from various concentration blends after PS removal. The Atomic Force Microscope (AFM) images clearly show two binodal decomposition regimes bridged by a spinodal decomposition-like appearance at 1:1 ratio. For high P3HT contents, porous films are obtained after PS removal. On the other hand, high content PS blends result in highly packed P3HT nanoislands when PS is selectively removed. Pore (island) diameter increases (decreases) with increasing PS content. Densities of pores or islands obtained are in the order of 10^6 pores or islands/mm^2. Interestingly, a P3HT wetting layer is obtained with the introduced method after removing PS, which suggests that the two polymers do also vertically phase separate during spin coating. Spectroscopic ellipsometry confirms the existence of the P3HT wetting layer next to the substrate before PS is removed (see below), which may be caused by a larger affinity between substrate and P3HT or related to the different solubilities of P3HT and PS in chlorobenzene. Table 1 summarizes the data collected from the AFM measurements. Larger scale AFM images and cross section profiles for 15, 25 and 35 PS wt% demonstrate a relatively high regularity on the pore diameter distribution (see Supporting Information).

Table 1: Different nanostructures obtained with P3HT:PS blends

PS (wt%)	15	25	35	50	65	75	85
Wetting layer	104	76	63	22	38	40	27
Depth/height	30	62	70	92	18	13	11
Pore diameter	120	200	335	-	-	-	-
Pore to pore	538	506	478	-	-	-	-
Island diameter	-	-	-	-	95	65	53
Island to Island	-	-	-	-	263	199	145

Average dimensions after PS removal calculated from the AFM images recorded in different parts of each film. All dimensions are expressed in nm. Pore (island) diameters are measured at half depth (height). The distances between pores or islands are measured from one center to the adjacent center.

In the literature, dichloromethane has been presented as a good solvent for PCBM while it leaves P3HT mostly undissolved.[9-11,21] This selectivity character of dichloromethane has been exploited here to obtain a simple solution process to produce P type – intermixed – N type (PiN) junctions by spin coating PCBM in dichloromethane on top of a P3HT thin film.[9-11] This method allows to obtain concentration gradient bilayer-like structures (or graded bilayers) that exhibit similar efficiencies as bulk heterojunctions.

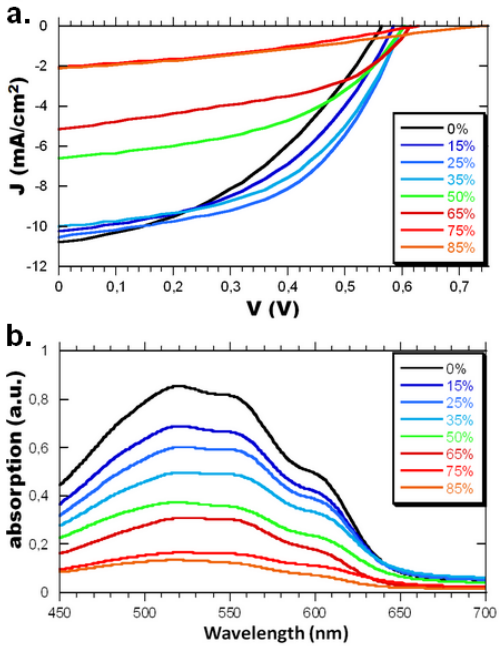

Figure 2. (a) J-V curves of devices obtained after PCBM deposition and (b) absorption spectra of the nanostructured films with various PS wt%.

Devices prepared using this method in our laboratory also exhibit similar efficiencies with respect to bulk heterojunctions. Dichloromethane swells the P3HT underlying layer allowing the PCBM to diffuse inside the P3HT chain network and creating a PCBM concentration gradient within the active layer. Previous results have suggested that the penetration of PCBM does not alter the packing of P3HT.[10] Creating nanostructured PiN junctions by simply spin coating PCBM from dichloromethane on top of the high surface roughness films obtained in our study should therefore give rise to active layers where both the Pi and iN interfaces are increased and therefore high device performances are expected. Moreover, organization of the P3HT chains in a favored direction due to nanoconfinement as well as interaction between the alkyl pending chains of P3HT (higher compatibility with respect to the polymer backbone) and PS may also favor the lying orientation or better pi-pi stacking of the P3HT chains in the blend thin films (i.e. more face-on oriented chains and less edge-on, which is normally found, see below).

Table 2: Performances of devices fabricated using nanostructured P3HT[a]

PS wt %	J_{sc} (mA/cm^2)	V_{oc} (V)	FF (%)	η (%)	R_s (Ω/cm^2)	Wetting layer (nm)	A/A_0[a]
0	10.8	0.57	41	2.51	7.04	130	1
15	10.2	0.60	46	2.77	8.27	104	0.832
25	10.5	0.61	51	3.25	4.61	76	0.745
35	10	0.61	49	3.02	4.18	63	0.640
50	6.6	0.61	47	1.89	5.05	22	0.473
65	5.1	0.62	45	1.43	17.84	38	0.361
75	2.0	0.65	32	0.43	7.69	40	0.217
85	2.1	0.74	30	0.47	28.57	27	0.162

Average properties of devices made after removal of PS, spin coating PCBM finalizing with 100 nm of Al and post annealing at 140˚C for 10 minutes inside a nitrogen filled glovebox.

a absorption ratio: ratio between integration of absorption of a given PS content (A) over absorption of pure P3HT spin coated film (A_0).

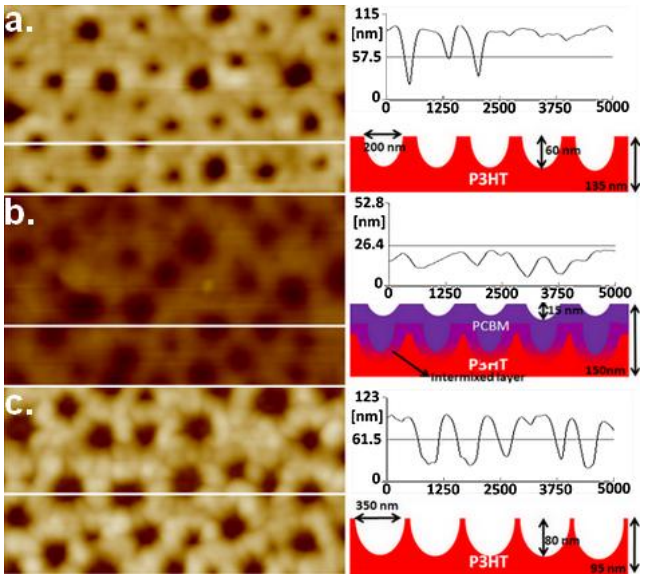

Figure 3. AFM images (5 µm x 2.75 µm), cross-section profiles and schematic representations of P3HT nanostructures (25 PS wt%) (a) before and (b) after coating with PCBM from dichloromethane and (c) after removing PCBM with cyclohexanone. The white lines in the AFM images indicate the place where the cross-section profiles were taken.

Devices were made using the previously presented nanostructured thin films by spin coating PCBM from dichloromethane solutions and evaporating aluminum cathodes. Current density-voltage curves are shown in Figure 2a for these structures compared to devices based on spin coated films of P3HT (graded bilayers). We note that the devices were prepared to optimize the conditions for nanostructured films; additional device optimization and characterization including changes in spin-coating and annealing conditions are discussed in the Supporting Information. As summarized in Table 2, the short circuit current decreases with increasing PS content beyond 35%, while the open circuit voltage increases. The first observation is partially due to the fact that the absorption is decreasing, as shown in Figure 2b. Interestingly, when normalizing the J_{sc} by the absorption, we note that the internal conversion of photons to electrons is more efficient on the nanostructured films reaching more than 50% efficiency increase for the blend prepared from 35% PS compared to the 0% PS.

Hence, other mechanisms, such as molecular reorientation or changes in crystallinity might be at the origin of the observed changes in J_{sc}. The tendency on V_{oc} could be explained if the introduction of PS interferes with the degree of crystallinity of the P3HT domains, making them smaller or reorienting them. We have observed, for instance, similar behavior when evaluating ternary solar cells based on regio regular P3HT, PCBM and regio random P3HT upon increasing the content of the amorphous polymer.[22] The fill factor, on the other hand, first increases up to 25-35 wt% PS content, and then decreases. The FF reaches up to 51% for 25 wt% PS, compared to a FF of 41% for the graded bilayers. One of the reasons that could lead to such an increase of the fill factor in an organic photovoltaic cell is the decrease of recombination of charges and the decrease of series resistance of the active layer. Both of these are often assigned to a better charge transport, which, on the other hand, are related to crystallinity increases in P3HT-based systems.[23] An increase in

contact selectivity between PEDOT:PSS and P3HT, as it may originate from the P3HT wetting layer acting somehow as a buffer layer, may also contribute to increase the fill factor. The initial increase in crystallinity with PS content suggested by the FF enhancement (and possibly on the normalized J_{sc}) seems in contradiction with the observed increase in V_{oc} indicating a more amorphous P3HT when introducing PS.

We therefore set out to try to understand which morphological changes are induced by PS nanostructuration and, as we will see, a possible explanation arises from changes in the orientation distribution of P3HT crystallites during the phase separation.

We start by investigating the P3HT:PCBM interface for nanostructured films. In order to explore this interface, we first spin coat PCBM from dichloromethane over the nanoporous films and then remove the PCBM layer by soaking the substrate into cyclohexanone (relatively good solvent for PCBM but non solvent for P3HT, as observed by an invariant morphology for pure P3HT soaked in cyclohexanone). We focus on the devices with PS wt% from 15 to 35 wt% as they give higher efficiencies compared to the graded bilayer. Figure 3 displays evidence of what is seen for films obtained with 25 wt% of PS: a 75% widening of the pores due to partial dissolution of the P3HT at the interface (further details with cross section profiles in the Supporting Information).

As P3HT has a low solubility in cyclohexanone, PCBM molecules embedded within the polymer chains may then be mediating the removal of P3HT from the film. These results suggest that a broad interface is obtained when spin coating PCBM from dichloromethane on top of the nanoporous P3HT layer (see diagram in Figure 3b). This interface, somewhere between 60 and 75 nm thick, is consistent with large charge generation rates as evidenced by the high photocurrent observed for the nanostructured films with low PS content. Moreover, the removal of P3HT by cyclohexanone seems to affect somehow more strongly the porous part of the film than the wetting layer, which may already indicate a different structure for the polymer chains in both regions, as we will see. Interestingly, for films containing 35 wt% of PS, after PCBM removal, we note that the pores not only widen but the thin layer between the pores tends to disappear resulting in films with a reduced surface roughness compared to the ones obtained with 25 wt% of PS. The small dimension porous films obtained with 15 wt% of PS give rise to almost flat surfaces after the PCBM spin coating process which indicates that, in this case, the pores are completely filled.

In order to further investigate the P3HT structure resulting from the demixing with PS, we have performed a detailed study using spectroscopic ellipsometry and FTIR on blend films deposited on glass and silicon before and after removal of the PS component. Effective medium approximation (EMA) analysis of the ellipsometric data (see details in the Experimental Section) for the blends allows characterizing the wetting and roughness layers. The obtained thicknesses for films supported on silicon wafers are around 10 nm for the wetting layer and about 4 nm for the roughness layer, almost independent of blend composition (for PS content lower than 50%), except for the 35% PS layer where the roughness increases up to 20 nm. This confirms the existence of the wetting layer.

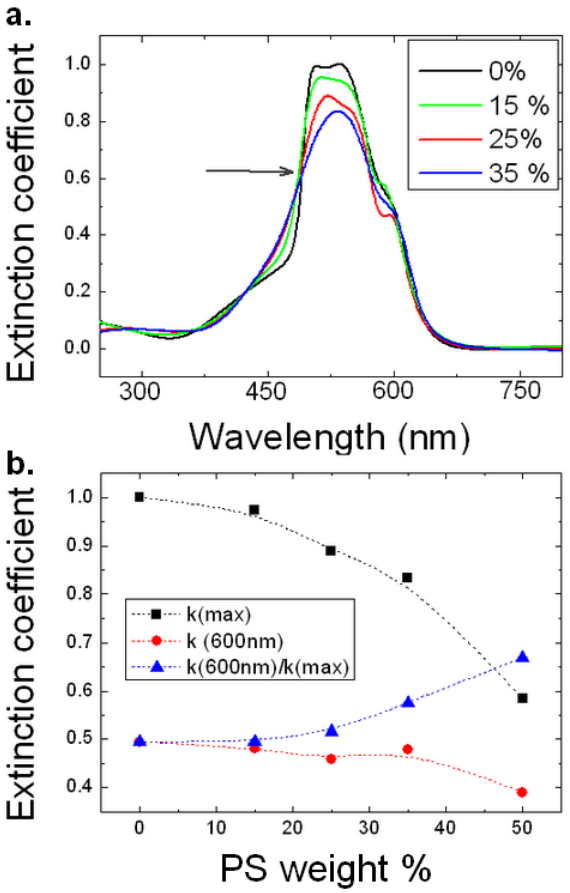

Figure 4. (a) Extinction coefficient of the P3HT domains within the P3HT:PS blend as a function of PS content deduced using the SCP model for the dielectric function of the domains mixed with PS via EMA model. The arrow points at the isosbestic point (490 nm). (b) Evolution with PS content of the maximum value of the extinction coefficient (squares), the extinction at 600 nm (circles) and the ration of the two (triangles).

We note that the ellipsometric data indicates that the thickness of the wetting layer increases upon PS removal.

In Figure 4, we show the evolution of extinction coefficient of the P3HT domains within the blend as a function of blend composition after refining the model above (see Experimental Section). The first observation is that the maximum absorption decreases with increasing PS content. As this is the absorption of the P3HT domains and not of the full film, this decrease cannot be ascribed to a lower content of P3HT molecules on the film, but to a lower average density or re-orientation of the domains. Moreover, part of the main absorption band is redistributed: there is a transfer of oscillator strength from long to short wavelengths through an isosbestic point (marked with an arrow in Figure 4a). As the absorption at lower wavelengths is associated with more amorphous material,[22] this would suggest that the P3HT domains are becoming more amorphous with increasing PS content and, possibly, crystallites are being re-oriented. This redistribution is also observed when normalizing the absorption data shown in Figure 2b. Interestingly, removing the PS results in a small reduction of the total film thickness, an enhancement of the maximum oscillator strength and a reduction of the partial void composition (with respect to the initial PS content). This suggests a relaxation of the structure upon PS removal (see also below).

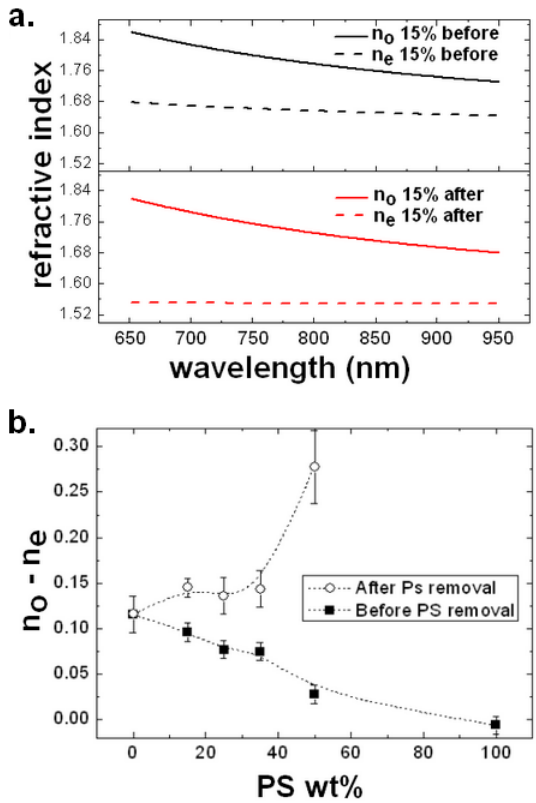

Figure 5. (a) Ordinary (solid lines) and extraordinary (dashed lines) indices of refraction in the transparency region for P3HT:PS (15 wt%) films before (top) and after (bottom) removal of PS; (b) PS concentration dependence of birefringence in P3HT:PS blends before (closed squares) and after (open squares) PS removal.

Another important observation is the increase of the intensity ratio between the P3HT crystal related shoulder at 600 nm and the absorption maximum (Figure 4b). This increase is consistent with an enhancement in the pi-pi stacking of P3HT chains.[24,25] Putting both arguments together, the ellipsometric analysis suggests that the P3HT domains are becoming more amorphous at the surface, which would explain the increase in V_{oc}, but simultaneously having greater pi-pi stacking, which may contribute to the increase in FF and absorption normalized photocurrent. This can be possible if a reorientation of the polymer chains is obtained with more backbones lying parallel to the substrate face on. A more amorphous upper part of the P3HT film could accommodate larger amounts of PCBM compared to a more crystallized wetting layer. This is fully consistent with the observation above of having a more effective removal of the polymer (75 nm) on the porous structure compared to the wetting layer (60 nm) when washing the PCBM covered nanostructure with cyclohexanone.

Changes in P3HT orientation were determined by fitting the transparent region of the ellipsometric spectra with an anisotropic model where the ordinary (parallel to surface, a.k.a in-plane) and extraordinary (perpendicular, a.k.a out-of-plane) refractive indices of P3HT were described with two independent Cauchy laws. Results are summarized in Figure 5. The obtained birefringence is a measure of the anisotropy and orientation of the polymer chains.

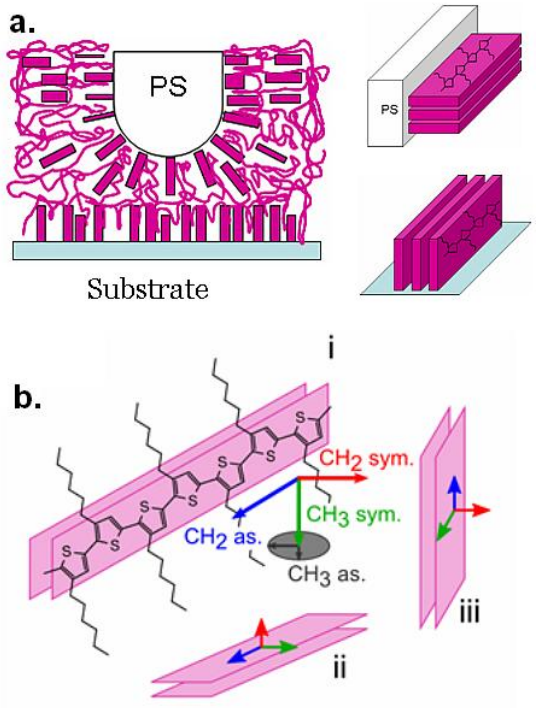

Figure 6. (a) Schematic representation of the P3HT chains orientation according to the ellipsometry analysis. (b) Schematic representation of mean dipole orientation relative to P3HT chain direction for the CH3 and CH2 stretching modes: i) corresponds to the observed orientation in pure P3HT films, ii) and iii) correspond to P3HT orientation compatible with the observed FTIR behavior.

The electronic dipole moment responsible for the main absorption band in P3HT is parallel to the polymer chains, which in spin coated films lay preferentially parallel to the substrate. As a consequence, P3HT films show negative birefringence ($n_{ordinary} > n_{extraordinary}$). With increasing PS composition, the birefringence decreases mainly because polystyrene is almost isotropic ($n_{ordinary} \leq n_{extraordinary}$) making the average effective dielectric function more isotropic. An indication of the blending effects on the P3HT domains is obtained from similar analysis on the blend films after removing the PS with acetone. Fits of the ellipsometric spectra of those films result in larger anisotropies for the P3HT:void mixture compared to the equivalent anisotropies with PS and even compared to the pristine P3HT film (0 wt% PS). This confirms the reorientation of the polymer chains more parallel to the substrate for the nanostructured films upon PS removal, which, together with the enhanced pi-pi stacking partially explains why the photocurrent is maintained and, simultaneously, the FF increased even though the P3HT domains are becoming more amorphous.

Taking into account the results from ellipsometry, the most probable orientation of the chains within the thin films and more specifically around the PS is schematically represented in Figure 6a. To support the proposed model, we use FTIR to probe the changes in molecular environment and orientation following the stretching modes of the P3HT side chains for the P3HT:PS blend samples.

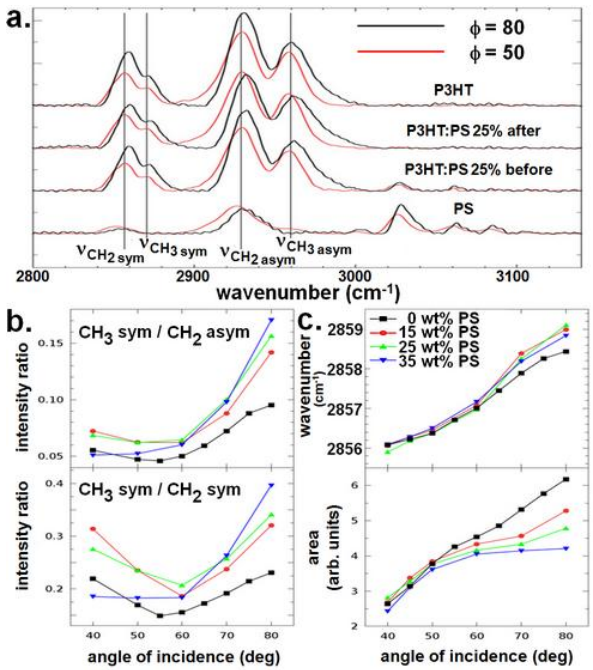

Figure 7. a) FTIR spectra at two angles of incidence (ϕ) of spin coated films of P3HT, PS, and a P3HT:PS blend (25 wt%) before and after removing PS. b) Composition and angle of incidence dependence of the CH2 symmetric mode energy (top) and peak area (bottom) after removing PS from the samples. (c) Composition and angle of incidence dependence of intensity ratio of the symmetric CH3 mode relative to the CH2 antisymmetric (upper part) and the CH2 symmetric (lower part) stretching modes intensities after removing PS from the samples.

Figure 7a shows absorption-like spectra in the 2800-3100 cm^{-1} region of the CH2 and CH3 vibrations, obtained from relative reflection spectra. First of all, the absence of specific PS absorption bands in the spectrum of P3HT:PS blend sample after PS removal confirms the suitability of acetone processing to produce nanoporous films without PS traces. In the P3HT and P3HT:PS blend, the symmetric CH_2 (~2857 cm^{-1}), symmetric CH_3 (~2871 cm^{-1}), asymmetric CH_2 (~2929 cm^{-1}) and asymmetric CH_3 (~2960 cm^{-1}) stretching modes are observed.

The electric dipole associated to each of these modes has a different orientation relative to the polymer backbone,[26] as illustrated in Figure 6b. Therefore, changes in energy and relative intensity of those modes may be used to gain information on changes in P3HT polymer crystallinity and orientation. To this purpose, the FTIR spectra for four compositions were fitted to a sum of Lorentzian lineshapes. Figure 7c shows the angle of incidence (AOI) and composition dependence of CH_3 symmetric stretching mode intensity relative to that of CH_2 stretching modes. The observed increase in CH3 intensity indicates a reorientation of the P3HT chains to situations that bring the symmetric CH3 vibration dipole more parallel to sample surface (schema ii and iii in Figure 6b). Of the two possibilities only ii is compatible with the increase in anisotropy derived from the ellipsometry results. The mode energy increases (Figure 7b) up to 3 cm^{-1} when going from 40 to 80 deg. Since larger AOI probe the close to surface region, the observed energy shift confirms the enhancement of the pi-pi stacking observed in ellipsometry.

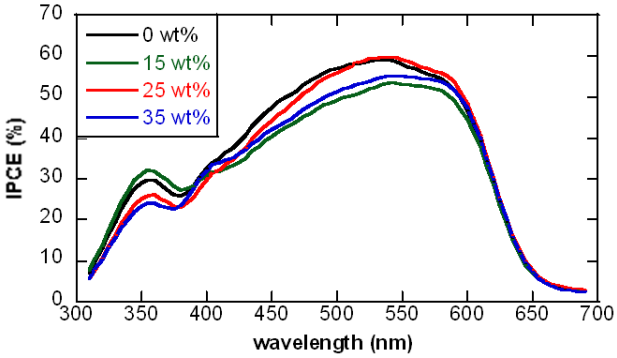

Figure 8: IPCE spectra of devices prepared using 0, 15, 25 and 35 PS wt% films

This enhancement, already present in the pure P3HT film, increases with the microstructure induced by PS blending and removal, providing an additional 1 cm^{-1} shift in the mode energy.

Combining the AFM images with the ellipsometric and FTIR data, we have established that the proposed processing scheme results in a PiN type active layer, with a P3HT wetting layer underneath (next to PEDOT:PSS) topped by an increased interface P3HT:PCBM mixed layer with enhanced pi-pi stacking of P3HT chains, and capped by a PCBM top layer.

To further understand the effect of the nanostructure dimensions as well as molecular reorientation, the incident photon-to-current efficiencies (IPCE) of samples obtained from blends with 0, 15, 25 and 35 PS wt% were measured (Figure 8). The IPCE of the various samples display notable changes. More specifically, we observe a slight increase of the PCBM contribution for the 15 PS wt% sample with respect to the planar P3HT reference. The PCBM contribution then decreases remarkably with increasing PS wt%. This can be directly related to the nanostructure formation. The small increase in interface in the 15 wt% films may explain the slightly larger contribution from PCBM as the pore radius in these films is still within the exciton diffusion range. On the other hand, the 25 and 35 PS wt% samples display nanopores with much larger dimensions (both radius and depth) making it less probable for an exciton created in the PCBM layer to reach a donor-acceptor interface.

The changes in the P3HT contribution to the IPCE spectra are equally interesting. As we observed previously, with increasing PS wt%, the amount of P3HT present in the active layers constantly decreases, and consequently, so does the absorption resulting from P3HT. Comparing the 0 and 15 PS wt% devices, this decrease in P3HT contribution related to absorption is present. However, the P3HT contribution is enhanced and red shifted in the 25 and 35 wt% samples. These films display enhanced pi-pi stacking which explains the red shift of the P3HT contribution in all nanostructured devices. Moreover, the better pi-pi stacking and molecular reorientation of the P3HT chains around the pore leads to better charge transport properties of the polymer in the vertical direction and therefore, charges can be extracted in a more efficient way in the nanostructured P3HT films. This is well in correlation with the IPCE spectra. The enhanced charge extraction originating from the reoriented P3HT chains induces both the red shift and the increase in the P3HT contribution.

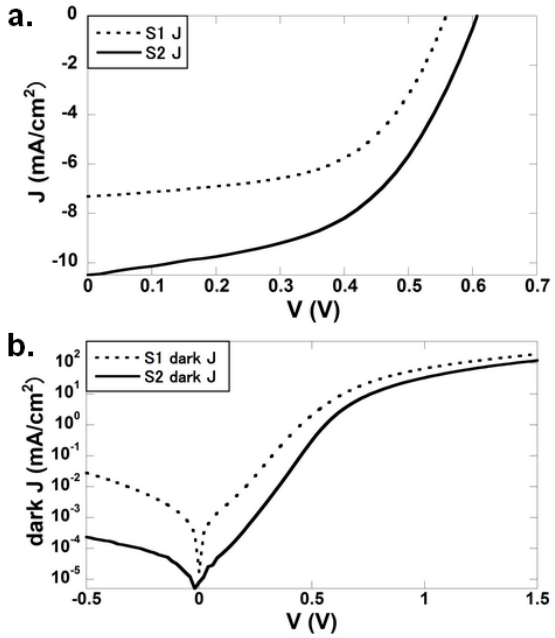

Figure 9. Comparative J-V (a) and dark J-V (b) curves of S1 and S2 type devices.

We next investigated the role of the wetting layer on the device performance. The wetting layer may have two opposite effects. A positive effect results from the P3HT wetting layer acting as electron blocking layer, thus enhancing the selectivity of the contact and consequently the FF. However, a thick wetting layer may severely increase series resistance beyond what is expected by making the film slightly more amorphous as it occurs in bulk heterojunctions when adding PCBM into P3HT. In terms of charge generation, thicker films would be more appropriate to absorb more light, but only if a polymer fullerene interface can be found within the exciton diffusion length, and so a compromise on the wetting layer thickness and nanostructured upper sublayer should be found to optimize the device performance.

In an effort to disentangle these effects, thinner nanostructured films were prepared. The aim was to obtain a similar nanostructure as the one previously obtained with 25 wt% of PS but with a thinner underlying wetting P3HT layer.

After a systematic investigation, we found that a similar structure, in terms of pore dimensions, was obtained by spin coating a 2:1 P3HT:PS blend (33 wt% of PS) at an increased spin coating speed (2000 rpm for 30s). Table 3 displays the average values obtained for devices with the same nanostructure but different thicknesses of wetting layers, namely, 25 wt% of PS spin coated at 1500rpm (S2 in the table, 76nm thick wetting P3HT layer) and 33 wt% of PS spin coated at 2000 rpm (S1 in the table, 43 nm thick wetting layer). As can be seen in Table 3 and Figure 9, the overall amount of P3HT decreases, therefore, less light is absorbed resulting in a lower J_{sc}. Normalizing the J_{sc} data by the absorption maximum, we note that the internal photon to electron conversion in these two samples is very similar.

Table 3: Wetting layer thickness vs series resistance (Rs)

	J_{sc}[a] (mA/cm²)	V_{oc} (V)	FF (%)	η (%)	R_s (Ω/cm²)	Wetting layer (nm)	A/A₀[b]
S1	7 (13.5)	0.57	56	2.19	3.33	43	0.52
S2	10.5 (14)	0.61	51	3.25	4.61	76	0.74

Average properties of devices made after removal of PS, spin coating PCBM finalizing with 100 nm of Al and post annealing at 140˚C for 10 minutes inside a nitrogen filled glovebox.

a corrected J_{sc} (in brackets) correspond to J_{sc} divided by the absorption ratio

b absorption ratio: ratio between integration of absorption of a given PS content (A) over absorption of pure P3HT spin coated film (A_0).

As predicted, J_{sc} and R_s decrease and FF increases as the wetting layer gets thinner. The FF increases from 51% to 56% as a consequence of the decrease in series resistance. Further decreasing the thickness of the wetting layer may result in the formation of leak points after PCBM spin coating as PCBM will diffuse all the way through the thin wetting layer to come into contact with PEDOT:PSS. However, comparing devices with two different wetting layer thicknesses, we demonstrate that FF up to 56% can be reached by engineering the thickness of both the wetting and nanostructured layers.

Further optimization by changing material properties (molecular weight, regio regularity etc) and processing conditions (temperature, solvent evaporation rate, etc) may lead to even more efficient devices if thin wetting layers can be produced underneath thick nanoporous upper layers.

Experimental section

P3HT (Mw = 21 000 g/mol) and PCBM were purchased from Merck and Luminescence Technology Corp, respectively. All solvents, as well as PS (Mw = 45 000 g/mol) were acquired from Sigma Aldrich and used as received. The PEDOT:PSS (Clevios P) used for the experiments was purchased from H.C. Starck.

Glass substrates coated with a 150 nm thick ITO layer were used as the anode. After a standard cleaning procedure, the substrates were exposed to UV irradiation in an UV-O_3 chamber and further covered with 45 nm of PEDOT:PSS (spin coated at 4000 rpm for 60s and further annealed at 200˚C for 10 min) which serves as a hole transporting and electron blocking layer in the photovoltaic devices.

Solutions of either pure P3HT or P3HT:PS blends were prepared at a concentration of 30 mg/ml in chlorobenzene and spin coated at either 1500 or 2000 rpm for 30 seconds on the ITO substrates (covered with PEDOT:PSS) resulting in film thicknesses of about 130-135 and 105-110 nm respectively. PS was removed from the P3HT:PS films by simply soaking the substrates into acetone for 30 minutes and further cleaning the film with some acetone to remove the remaining PS from the surface. Complete PS removal was confirmed by FTIR measurements. The resulting thin films of P3HT exhibit various nanostructures. The pure and nanostructured layers of P3HT are then covered with a solution of PCBM in dichloromethane (10 mg/ml) spin coated at 2000 rpm for 30 seconds. The resulting active layer thickness is around 150 nm for the P3HT:PS blends spin-coated at 1500 rpm and 130 nm for the ones spin-coated at

2000 rpm.

Film thicknesses were measured by scratching the film and measuring the height difference across the scratch using an AFM from Keyence (Nanoscale Hybrid Microscope VN-8000). The same AFM apparatus was also used to characterize the morphology of the nanostructures. Absorption spectra were measured using a Jasco V670 UV/Vis Spectrometer.

All devices were finalized by evaporating a 100 nm thick Aluminium cathode under vacuum (10^{-6} Torr) and encapsulated with a glass cap using an ultraviolet curing epoxy resin inside a nitrogen filled glovebox. The active areas were shadowed during the 15-min exposure to the UV radiation to avoid photodegradation of the organic layers. The active area of the devices was defined to 2 mm^2 by the overlapped area of the ITO and Al electrodes.

The current–voltage characteristics of the encapsulated devices were measured in air, using a Keithley 2400 Sourcemeter and a Solar simulator at one sun light irradiance (AM 1.5, 100mW/cm^2) at room temperature. IPCE measurements were obtained using encapsulated devices and measuring Isc and input power for each monochromated incoming excitation.

Spectroscopic ellipsometry measurements were performed with a rotating polariser GES5E system with CCD detection from SOPRALAB on P3HT:PS blends before and after PS removal for films deposited onto glass and silicon substrates. Spectra between 1.22 and 5 eV were taken at several angles of incidence between 55 and 75 degrees. Ellipsometry measures reflection induced changes in light polarization. For thin film samples, these changes are usually described by a multilayer model with the appropriate number of layers, whose thicknesses and optical properties are adjustable parameters.[27] Fitting the model to measured spectra provides information on the film optical, geometrical and morphological properties. Three different models were used to evaluate the morphology of the films, namely, an effective approximation model, a full description of the dielectric function using the standard critical point model, and an anisotropic model in the transparent region. Before analyzing the ellipsometry spectra of the blend films, we first obtained the optical constants of the constituents. For this, ellipsometric spectra of films of pure P3HT and PS were fitted to models consisting of a film on a silicon substrate. Polystyrene spectra were described with a Cauchy dispersion law and P3HT with a Standard Critical Point model (SCP).[28] The obtained optical functions were then used to analyze the spectra of the blend films.

For the P3HT-PS blend films, the best EMA model fits were obtained with a three layer model consisting of a wetting layer of P3HT, the blend layer and a roughness layer on top of the Si/SiO2 substrate. As a first step, we assume that the optical properties of P3HT do not change upon mixing. Thus, the blend and roughness layers are modeled with a Bruggeman EMA, with composition parameter values fitted for the blend and fixed at 50% void for the roughness layer. Additional information on the blending induced changes was obtained with an improved model. Fixing the layer thickness and PS composition of the previous EMA model, we fit at each blend composition the SCP model parameters that describe the dielectric function of the P3HT domains within the blend. A final model was developed in order to assess the changes in polymer orientation. For this, an anisotropic model consisting of two Cauchy laws, one in plane and the other out of plane was fitted across the transparency region of the materials.

We note that, although qualitatively in agreement, there are some quantitative differences between the ellipsometrically deduced parameters and the AFM and absorption measurements. This is partially due to the use of different substrates that yield different film thickness and morphologies. With respect to absorption deduced from transmission data, we also note the fact that with ellipsometry we are modeling the P3HT domains which are embedded within the PS matrix, while the absorption data shown correspond to the whole film and neglects the reflected and scattered light.

FTIR spectra were measured in a Vertex 70 system from Bruker using a variable angle reflection accessory and a mid-band MCT detector. Using the normal incidence spectrum as reference, spectra from 750 to 3300 cm^{-1} were measured at different angles of incidence (40-80 degrees). For each sample, unpolarized spectra taken at several angles of incidence are divided by a reference spectrum taken at near normal incidence on the same sample. In this way, we obviate possible errors due to sample size, shape and dispersion differences. In reflection spectra the absorption bands appear as dips on a smooth varying background. The spectra shown below were produced by subtracting that background and inverting the result.

Conclusions

In summary, we demonstrate that high efficiency nanostructured solar cells can be obtained by simple solution processes which do not involve the use of soft lithography or elaborated chemical modifications. By using a blend of two commercially available polymers and selectively removing one of the phases, thin films of nanoporous P3HT are obtained. These films are used to produce high interface PiN junctions which show enhanced fill factors and efficiencies compared to bulk heterojuntions and planar PiN geometries. More specifically, the interdigitated PiN junction exhibits an efficiency increase of up to 29 % with respect to the graded bilayer. These enhancements are rationalized in terms of the resulting structure, namely a P3HT wetting layer topped by an interdigitated mixed P3HT:PCBM middle layer with enhanced pi-pi stacking of polymer chains and increased free volume to accommodate a higher content of fullerene molecules, and all topped with a PCBM layer. Furthermore, we have demonstrated that, although the efficiency gets lower as less photons are absorbed, by simply decreasing the series resistance of the devices using a thinner wetting layer, the FF can further increase up to 56%. Our results demonstrate that, even though most of the research is oriented towards elaborated systems to obtain nanostructured thin films of P3HT, simple techniques based on solution processes can lead to a fast and easy way to produce efficient nanoarchitectures in solar cells. Self assembled processes also induce effects that cannot be obtained with soft lithography: along with the increase of the interface due to the nanostructures, the arrangement of the P3HT chains around the PS filled pores is one of the key parameter to increase the efficiency of the bilayer solar cells. Interestingly, crystallinity is not a prerequisite of the polymer semiconductor for this

technique to work, so it can easily be extended to novel low band gap polymers. While recent research is mainly focusing on elaborated and costly fabrication methods to produce highly organized devices, we have demonstrated that simple methods also have the potential to create multilevel organization (nanomorphology and molecular level) enhanced efficiency devices. Furthermore, as this process is both cost effective and based on commercially available polymers, it could be easily transferred to industrial production.

Notes and references

[a] *Japan Advanced Institute of Science and Technology (JAIST), School of Materials Science, 1-1 Asahidai, Nomi, Ishikawa 923-1292, Japan*
Tel: +81-761-51-1531; Fax: +81-761-51-1149;
E-mail: varunvohra1984@gmail.com, murata-h@jaist.jp.ac
[b] *Institut de Ciència de Materials de Barcelona (ICMAB-CSIC), Campus de la Universitat Autònoma de Barcelona, E-08193 Bellaterra, Catalonia, Spain; E-mail: mcampoy@icmab.es, miquel@icmab.es*

† Electronic Supplementary Information (ESI) available: [AFM large scale and profile cross-sections of nanostructured P3HT; discussion on device optimization]. See DOI: 10.1039/b000000x/

‡ The work was supported by a Grant-in-Aid for Scientific Research on Innovative Areas (No. 20108012, "pi-Space") from the Ministry of Education, Culture, Sports, Science, and Technology, Japan. V. Vohra would like to greatly acknowledge financial support through research fellowships from the Japan Society for Promotion of Science for postdoctoral fellowships for foreign researchers. The authors also acknowledge the Spanish Ministry of Economy and Competitiveness for generous funding through projects PLE2009-0086 and MAT2009-10642.

1 A. C. Mayer, S. R. Scully, B. E. Hardin, M. W. Rowell, M. D. McGehee, *Materials Today*, 2007, **10**, 28-33.
2 N. Camaioni, G. Ridolfi, G. Casalbore-Miceli, G. Possamai, M. Maggini, *Adv. Mater.*, 2002, **14**, 1735-1738.
3 F. Padinger, R. S. Rittberger, N. S. Sariciftci, *Adv. Funct. Mater.*, 2003, **13**, 1-4.
4 D. Chirvase, J. Parisi, J. C. Hummelen, V. Dyakonov, *Nanotechnology*, 2004, **15**, 1317-1323.
5 M. Reyes-Reyes, K. Kim, D. L. Carroll, *Appl. Phys. Lett.*, 2005, **87**, 083506.
6 W. Ma, C. Yang, X. Gong, K. Lee, A. J. Heeger, *Adv. Funct. Mater.*, 2005, **15**, 1617-1622.
7 G. Li, V. Shrotriya, J. Huang, Y. Yao, T. Moriarty, K. Emery, Y. Yang, *Nature Mater.*, 2005, **4**, 864-868.
8 A. Kumar, G. Li, Z. Hong, Y. Yang, *Nanotechnology*, 2009, **20**, 165202.
9 D. H. Wang, H. K. Lee, D.- G. Choi, J. H. Park, O. O. Park, *Appl. Phys. Lett.*, 2009, **95**, 043505.
10 A. L. Ayzner, C. J. Tassone, S. H. Tolbert, B. J. Schwartz, *J. Phys. Chem. C*, 2009, **113**, 20050–20060.
11 K. H. Lee, P. E. Schwenn, A. R. G. Smith, H. Cavaye, P. E. Shaw, M. James, K. B. Krueger, I. R. Gentle, P. Meredith, P. Burn, *Adv. Mater.*, 2011, **23**, 766-770.
12 M. Aryal, F. Buyukserin, K. Mielczarek, X.- M. Zhao, J. Gao, A. Zakhidov, W. Hu, *J. Vac. Sci. Technol. B*, 2008, **26**, 2562-2566.
13 W. Wiedemann, L. Sims, A. Abdellah, A. Exner, R. Meier, K. P. Musselman, J. L. MacManus-Driscoll, P. Müller-Buschbaum, G. Scarpa, P. Lugli, L. Schmidt-Mende, *Appl. Phys. Lett.*, 2010, **96**, 263109.
14 J. S. Kim, Y. Park, D. Y. Lee, J. H. Lee, J. H. Park, J. K. Kim, K. Cho, *Adv. Funct. Mater.*, 2010, **20**, 540-545.
15 K. Sivanandan, T. Chatterjee, N. Treat, E. J. Kramer, C. J. Hawker, *Macromolecules*, 2010, **43**, 233-241.
16 A. Takahashi, Y. Rho, T. Higashihara, B. Ahn, M. Ree, M. Ueda, *Macromolecules*, 2010, **43**, 4843-4852.
17 X. Han, X. Chen, S. Holdcroft, *Adv. Mater.*, 2007, **19**, 1697-1702.
18 F. A. Castro, H. Benmansour, C. F. O. Graeff, F. Nuesch, E. Tutis, R. Hany, *Chem. Mater.*, 2006, **18**, 5504-5509.
19 M. Campoy-Quiles, T. Ferenczi, T. Agostinelli, P. G. Etchegoin, Y. Kim, T. D. Anthopoulos, P. N. Stavrinou, D. D. C. Bradley, J. Nelson, *Nature Mater.*, 2008, **7**, 158-164.
20 J. Jaczewska, A. Budowski, A. Bernasik, E. Moons, J. Rysz, *Macromolecules*, 2008, **41**, 4802-4810.
21 B. Tremolet de Villers, C. J. Tassone, S. H. Tolbert, B. J. Schwartz, *J. Phys. Chem. C*, 2009, **113**, 18978-18982.
22 M. Campoy-Quiles, Y. Kanai, A. El-Basaty, H. Sakai, H. Murata, *Org. Electron.*, 2009, **10**, 1120-1132.
23 V. D. Mihailetchi, H. Xie, B. de Boer, L. J. A. Koster, P. W. M. Blom, *Adv. Funct. Mater.*, 2006, **16**, 699-708.
24 J. Clark, J.- F. Chang, F. C. Spano, R. H. Friend, C. Silva, *Appl. Phys. Lett.*, 2009, **94**, 163306.
25 U. Zhokhavets, T. Erb, G. Gobsch, M. Al-Ibrahim, O. Ambacher, *Chem. Phys. Lett.*, 2006, **418**, 347-350.
26 P. E. Laibinis, G. M. Whitesides, D. L. Allara, Y. T. Tao, A. N. Parikh, R. G. Nuzzo, *JACS*, 1991, **113**, 7152-7167. (Table II)
27 R. M. A. Azzam, N. M. Bashara, *Ellipsometry and Polarized Light (Elsevier)*, 1977.
28 M. Campoy-Quiles, J. Nelson, D. D. C. Bradley, P. G. Etchegoin, *Phys. Rev. B*, 2007, **76**, 235206.

Supplementary Information

Organic Solar Cells Based on Nanoporous P3HT Obtained from Self Assembled P3HT:PS Templates

Varun Vohra, Mariano Campoy-Quiles, Miquel Garriga and Hideyuki Murata

In the Supporting Information, we provide further characterization of the nanostructured films and devices obtained based on these films.

More specifically, AFM depth profiles as well as larger scale AFM images of the nanostructured obtained with 15, 25 and 35 PS wt% are displayed in Figure SI1. With this insight of the structures obtained, we can appreciate in a better way the pore regularity on a larger area.

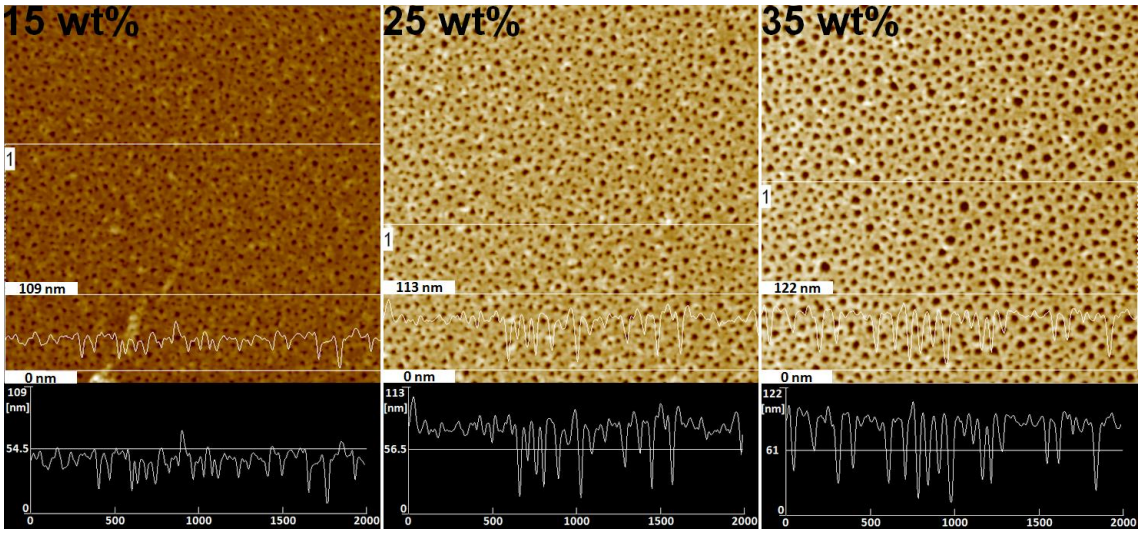

Figure SI1. 20 x 20 μm AFM images of the nanostructures obtained with 15, 25 and 35 PS wt% and their corresponding cross-section profiles.

These structures are obtained specifically with the chosen molecular weights (Mw) for both P3HT and PS. The low Mw P3HT used for the experiments is well adapted for device fabrication but higher Mw P3HT such as the ones used in literature may result in higher performances (reaching up to 3.5% of efficiency in average).[SI1,SI2]

For a better understanding of our choice for the device architecture, more specifically, for the choice of the cathode (only aluminum unlike the calcium/aluminum electrode used in literature),[SI1,SI2] we provide further comparison with the state-of-art of

the graded bilayer devices. As can be seen in the main article, our reference device does not display efficiencies as high as 3.5 %. This is related to a few limitations resulting from the use of a P3HT with specific Mw (21 000 g/mol). Unlike the P3HT used in literature (Mw = 45 000 g/mol), we cannot anneal the thin films prior to electrode deposition as this results in much lower efficiencies. P3HT may migrate in the vertical direction through similar pre-annealing and with the low Mw P3HT used in our work, there is a larger probability to observe such migration. Unlike Ca/Al, using only Al allows post-annealing the devices which then exhibit much higher performances than the pre-annealed ones with Ca/Al as the top electrode. We also optimized the post-annealing conditions to get good reproducibility with a post-annealing of 140°C for 10 min. Results using an annealing temperature of 150°C for 10 min demonstrate better device performances for about half the devices but the remaining half display a remarkable decrease in fill factor (FF) leading to lower efficiencies. In Table SI2, we summarize the performances of devices obtained with efficient annealing.

As this work is a proof of concept regarding the influence of the pore dimensions over the device performances, we chose the spin-coating conditions (P3HT:PS blends spin-coated at 1500 rpm for 30s) that provides the widest range of pore dimensions. Furthermore, the use of high boiling point solvents such as dichlorobenzene is known to give better performances but no nanoporous structures are obtained if dichlorobenzene is used as the solvent. Last but not least, in order to fill the pores as much as possible, the optimized conditions for PCBM spin-coating (4000 rpm for 10s) were modified. We choose to spin-coat the PCBM solution in dichloromethane (10 mg/ml) at 2000 rpm for 30s. However, in Table SI2, we find the comparison between both PCBM spin coating conditions.

PS wt%/PCBM spin-coating speed	Jsc (mA/cm^2)	Voc (mV)	FF (%)	PCE (%)
0 wt% / 2000 rpm	10.0	591	46.6	2.75
0 wt% / 4000 rpm	9.79	604	50.7	2.99
15 wt% / 2000 rpm	9.09	602	53.8	2.95
15 wt% / 4000 rpm	8.81	610	57.9	3.12
25 wt% / 2000 rpm	10.0	611	54.3	3.32
25 wt% / 4000 rpm	9.26	611	56.4	3.19
35 wt% / 2000 rpm	9.67	619	54.6	3.27
35 wt% / 4000 rpm	8.14	612	59.9	2.98

Table SI2: summary of the device performances obtained under various conditions. All devices are post-annealed at 150°C for 10 min.

As we can observe inTable SI2, the device performances greatly depend on the

PCBM deposition conditions. Theoretically, while the faster spinning condition (4000 rpm) leads to enhanced photovoltaic performances for the low surface roughness P3HT films (up to 15 wt%), the slower spinning condition (2000 rpm) allows a better filling of the porous structures resulting in higher efficiencies for the 25 and 35 PS wt% films. Interestingly, as we can see in Figure SI2, the device performances perfectly follow these trends.

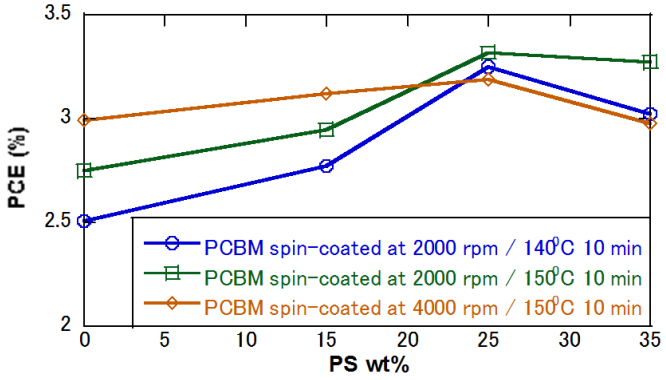

Figure SI2. Evolution of the PCE with increasing PS wt% from device fabricated under various conditions, namely, with PCBM spin-coated at either 2000 rpm (blue and green) or 4000 rpm (red) and the resulting devices annealed at either 140°C (blue) or 150°C (green and red).

Throughout literature on graded bilayer structures, the reproducibility of the results seems to be a major issue (maximum efficiencies of 3.8 % with an average of 3.5 % for similar conditions).[SI1,SI2] In the main text of our work, we focus on obtaining reproducible results (annealing at 140°C for 10 min) and chose the optimized conditions for nanostructured devices. To be able to compare the influence of nanostructures over the device performances, we compare them to devices obtained in the same conditions. However, the optimized nanostructured devices even overcome the performances of the optimized planar devices as the pores obtained (e.g. for the 25 PS wt% films) are partially filled during the spin-coating process.

References (Supporting Information):

(SI1) A. L. Ayzner, C. J. Tassone, S. H. Tolbert, B. J. Schwartz, *J. Phys. Chem. C*, 2009, **113**, 20050–20060.

(SI2) K. H. Lee, P. E. Schwenn, A. R. G. Smith, H. Cavaye, P. E. Shaw, M. James, K. B. Krueger, I. R. Gentle, P. Meredith, P. Burn, *Adv. Mater.*, 2011, **23**, 766-770.